Session 2A: MODES
Extracting eigenmode frequencies

Comm. in Asteroseismology
Vol. 157, 2008, Wrocław HELAS Workshop 2008
M. Breger, W. Dziembowski, & M. Thompson, eds.

Extracting oscillation frequencies from sparse spectra: Fourier analysis

M. Jerzykiewicz

Instytut Astronomiczny, Uniwersytet Wrocławski,
Kopernika 11, 51622 Wrocław, Poland

Abstract

I begin by explaining the properties of spectral windows of time-series data. Emphasis is on data obtained at a single geographic longitude, but ground-based multi-longitude campaigns and space missions such as MOST and Hipparcos are not entirely neglected. In the second section, I consider the Fourier transform of time-series data and the procedure of pre-whitening. Sect. 3 is devoted to the pioneers of the subject. In Sect. 4, I suggest how to avoid pitfalls in the practice of periodogram-analysing variable-stars observations. In the last section, I venture an opinion.

Individual Objects: AR Her, δ Cet, β CMa, δ Sct, DD Lac, EN Lac, 2 And

Spectral windows

Spectral windows, also called window functions, are Fourier transforms of the observing windows. For a single site, the proof is illustrated in Fig. 1. This figure is a slight modification of figure 3-7 from the well-known monograph by Gray (1976). In the monograph, the figure serves to explain the working of a diffraction grating. In Fig. 1, the observing window is shown at top left, and its Fourier transform, at top right. The observing window consists of nine successive nights, equally spaced, each of duration Δt. It can be looked at as a result of a convolution of a rectangular function of width Δt (representing a single night) with a Shah function with spacing equal to the sidereal day, T_*, multiplied by another rectangular function of width T, equal to the total time-span of the observations. This wide rectangular function transforms into the narrow sinc function of width $1/T$ (bottom right), while the single-night rectangular function transforms into the wide sinc function of width $1/\Delta t$ (upper right). The latter, multiplied by the Shah function with spacing equal to $1/T_*$ (the transform of the Shah function at left) and convolved with the former gives the spectral window. Note that (1) the frequency resolution is determined by T, the total time-span of the data, and (2) $1/T_*$ is equal to one cycle per sidereal day (c/sd), i.e., 1.0027 c/d.

In Fig. 1, the diagram at lower left and all diagrams at right (i.e., in the frequency domain) are incomplete. In fact, the sinc and Shah functions extend from $-\infty$ to $+\infty$. In particular, the spectral window (top right) is a sum of an infinite series of the narrow sinc functions, spaced 1 c/sd, with their maximum ordinates modulated by the wide sinc function. The pattern has a maximum at zero frequency. Note that the duration of the observing night, Δt, determines the height of the -1.0027 and $+1.0027$ c/d side-lobes relative to the central peak: longer nights produce lower side-lobes.

The observing window in Fig. 1 (top left) is grossly simplified. I assumed that (1) on any night, the observations are taken continuously, (2) the nights are of equal duration, (3) there are no nights lost because of clouds or equipment failure. The first assumption was made to

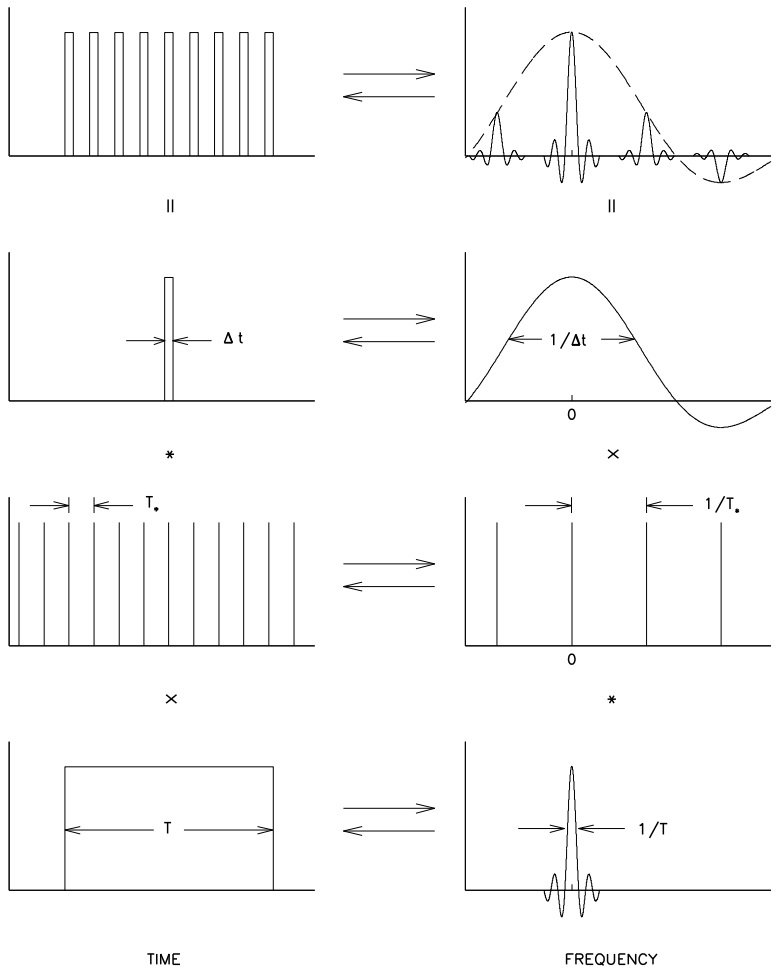

Figure 1: The spectral window (top right) is the Fourier transform of the observing window (top left). The observing window is a result of a convolution of a rectangular function of width Δt (representing a single night) with a Shah function with spacing equal to the sidereal day, T_*, multiplied by another rectangular function of width T, equal to the total time-span of the observations. The spectral window is a convolution of the narrow sinc function of width $1/T$ (bottom right) with the Shah function of spacing equal to $1/T_*$ (the transform of the Shah function at left) multiplied by the wide sinc function of width $1/\Delta t$ (upper right)

avoid discussing the Nyquist frequency, an issue which for irregularly spaced time series seems to be debatable (see Koen 2006). Assumptions (2) and (3) make the observing window an even function of time, so that the spectral window is a real (and even) function of frequency. For actual data, the spectral window is a complex function. In practice, one plots the modulus of the spectral window. The modulus of a spectral window is an even function of frequency.

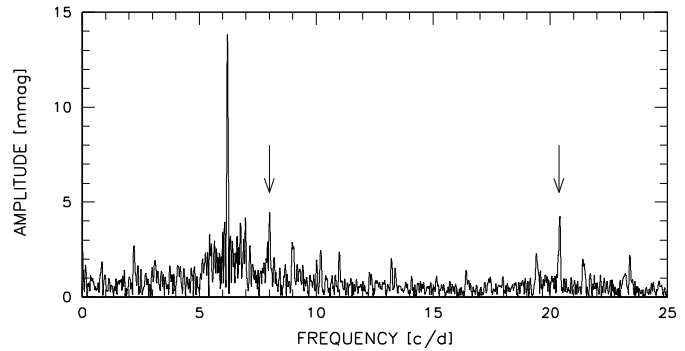

Figure 2: Synthetic amplitude spectrum of the MOST observations of δ Cet. The arrows indicate aliases at $f_{orb}-$ 6.2059 and f_{orb} + 6.2059 c/d, where $f_{orb} = 14.20$ c/d is the orbital frequency of the satellite

An interesting example of how much a real spectral window may differ from the simplified case discussed above can be found in Borkowski's (1980) analysis of visual observations of the RRab-type Blazhko variable AR Her, obtained in 1944 by Tsessevich. In the spectral window of these data (Borkowski's figure 1) one can see not only the peak at zero frequency and the 1, 2, 3 etc. c/sd aliases, but also a peak at the star's fundamental frequency of 2.128 c/d and its sidereal day aliases. This latter pattern arose because Tsessevich has spaced his observations unevenly: the sharp light-maxima he sampled with a much shorter time step than the flat minima.

The sidereal day aliases can be reduced or even eliminated altogether by observing from several sites at different longitude or from space. An example of a multi-longitude ground-based spectral window can be seen in the top panel of figure 2 of Handler et al. (2004), while an example of a space-based spectral window is shown in Fig. 2. Strictly speaking, both figures show moduli of the Fourier transforms of synthetic data, produced by sampling a sine-curve that represents the highest-amplitude variation of the star in question at the epochs of actual observations. In order to avoid confusion with the spectral windows proper, I shall refer to the former as "the synthetic spectra". The synthetic spectrum in Fig. 2 was computed for the 6.2059 c/d variation of the β Cephei-type star δ Cet; the synthetic data were produced by sampling a 13.8 mmag sine-curve of this frequency at the epochs of the MOST[1] photometric observations of the star. The figure shows the 13.8 mmag peak at 6.2059 c/d and, in addition, much lower peaks at $f_{orb}-$ 6.2059 and $f_{orb}+$ 6.2059 c/d, where $f_{orb} = 14.20\ c/d$ is the orbital frequency of the satellite. For a detailed discussion of ground-based and MOST observations of δ Cet, see Jerzykiewicz (2007).

In the Hipparcos' (ESA 1997) epoch photometry, the satellite's rotation-frequency aliases are more pronounced than the orbital-frequency aliases in the MOST observations of δ Cet. In addition, the amplitude of the aliases is modulated with a frequency resulting from beating between the two sampling frequencies of the satellite. A thorough discussion of the spectral window of the Hipparcos' epoch photometry has been provided by Jerzykiewicz & Pamyatnykh (2000).

[1] The MOST satellite is a Canadian Space Agency mission, jointly operated by Dynacon Inc., the University of Toronto Institute for Aerospace Studies and the University of British Columbia, with the assistance of the University of Vienna.

Fourier transform of the observations and pre-whitening

Time-series observations of a variable star can be represented as a sum of (1) the product of the star's intrinsic variation and the observing window, and (2) the observational noise. From the convolution theorem and the fact that the Fourier transform of a sine-curve of frequency f is a pair of the δ functions, one placed at $-f$, and the other, at $+f$, it follows that:

T1 If the intrinsic variation is a sine-wave of frequency f and amplitude A, the Fourier transform of the observations is equal to the sum of (1) the spectral window shifted to $-f$, (2) the spectral window shifted to $+f$, and (3) the Fourier transform of the observational noise; (1) and (2) are scaled to A.

T2 If the intrinsic variation is a sum of N sine-waves, the Fourier transform of the observations is equal to the sum of N of (1), N of (2) and (3).

In practice, one plots the moduli of the Fourier transforms. T1 explains the orbital-frequency aliases in Fig. 2, in particular, the alias at $f_{orb}-$ 6.2059 c/d. T2 makes it clear why pre-whitening is necessary if more than one frequency is present in the variation. If done in the time domain, as is usually the case, pre-whitening is an operation on real numbers. In the frequency domain, the real and the imaginary part of the transform must be treated. An example of pre-whitening in the time domain can be found in Handler et al. (2004). Pre-whitening in the frequency domain has been advocated by Gray & Desikachary (1973).

The pioneers

Meyer (1934) discovered that the radial velocity amplitude of the β Cephei-type star β CMa varied with a period equal to 49.1 d. He explained this in terms of an interference between two sine-curves of slightly different short periods, one equal to $6^h\,0^m$, the other, to $6^h\,2^m$. The reality of the components was supported by the fact that the longer of the two short periods was identical with the period of the variation of the width of spectral lines, discovered earlier by Henroteau (1918).

Sterne (1938) applied the correct procedure of pre-whitening (without using the term) in order to derive a secondary period of δ Sct from photoelectric observations of Fath (1935, 1937).

Fath (1947) made an (unsuccessful) attempt to organize a multi-longitude campaign; the intended object was the β Cephei-type star 12 (DD) Lac. His secondary period of 12 Lac, derived from a single-longitude data, was later shown to be a $\sim$1 c/sd alias of the correct value. In 1956, de Jager (1963) organized the first successful multi-longitude campaign; the object was again 12 Lac.

Wehlau & Leung (1964) explained periodogram analysis in terms of Fourier transform and the convolution theorem.

Fellgett (1972) discussed limitations of periodogram analyses of time-series observations. He pointed out that (1) the existence of a Fourier component does not of itself provide any evidence of significant periodicity, (2) there is no unique Fourier representation of a function known over a finite interval of its argument. According to the NASA's ADS, Fellgett's (1972) important paper has been quoted only once. Apparently, Cassandras are unpopular.

Recommendations

This section should be skipped by those who do not make mistakes. The less fortunate among us may wish –before sending the results of their analysis to the editor– to go through the following list:

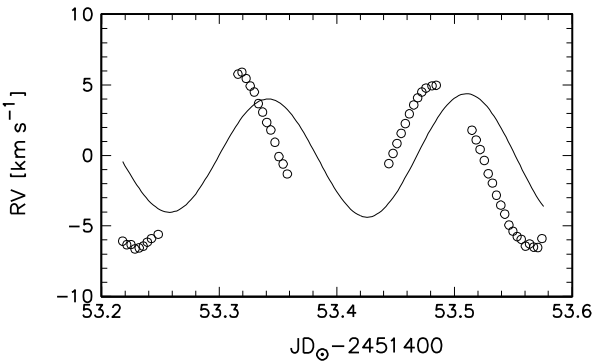

Figure 3: The radial-velocity observations (circles) and synthetic velocity-curve (solid line) of 16 (EN) Lac on JD 2451453. The observations and parameters of the synthetic curve are from Lehmann (2001). The synthetic curve was computed by MJ.

- Get the epochs of observations right. However, if you are lucky, your mistake may surface during the analysis. For an example, see figure 5 in Jerzykiewicz & Wenzel (1977).
- If you do differential photometry, use two (or more) comparison stars. A single comparison star may spoil the analysis. Example: I ascribed the frequency of 7.194 c/d to 16 (EN) Lac (Jerzykiewicz 1993). As it turned out, it was 2 And, the only comparison star I used, which is responsible (Sareyan et al. 1997, Handler et al. 2006).
- Understand the spectral window of your data. See Sect. 1.
- Pre-whiten. See Sect. 2.
- Quit before you get too close to the level of noise. See Breger et al. (1999).
- Compare the synthetic light (or velocity) curve with the data. If you don't, you risk an unpleasant surprise. An example is shown in Fig. 3.
- When you compare the frequencies you derived with earlier work, look for differences close to 1.003 and 0.003 c/d. The first number is approximately equal to 1 c/sd (see Sect. 1), the second is close to 1 cycle per year (c/y). An alias of 1 c/y (or a fraction thereof, such as 1/2, 1/3, etc.) is much more difficult to get rid of than a 1 c/sd alias.

An opinion

If the data are OK, any method of analysis will do, provided that the method is used properly.

Acknowledgments. The use of NASA's Astrophysics Data System Abstract Service is acknowledged. This work was supported by MNiSW grant N203 014 31/2650.

References

Borkowski, K. J. 1980, AcA, 30, 393
Breger, M., Handler, G., Garrido, R., et al. 1999, A&A, 349, 225
ESA 1997, The Hipparcos and Tycho Catalogues, ESA SP-1200
Fath, E. A. 1935, LicOB, 17, 175
Fath, E. A. 1937, LicOB, 18, 77
Fath, E. A. 1947, PGooO, 12, 3
Fellgett, P. 1972, Ap & SS, 16, 437
Gray, D. F. 1976, The Observation and Analysis of Stellar Photospheres, Wiley, New York
Gray, D. F. & Desikachary, K. 1973, ApJ, 181, 523
Handler, G., Jerzykiewicz, M., Rodrguez, E., et al. 2006, MNRAS, 365, 327
Handler, G., Shobrook, R. R., Jerzykiewicz, M., et al. 2004, MNRAS, 347, 454
Henroteau, F. 1918, LicOB, 9, 155
Jager, C. de 1963, BAN, 17, 1
Jerzykiewicz, M. 1993, AcA, 43, 13
Jerzykiewicz, M. 2007, AcA, 57, 33
Jerzykiewicz, M., & Pamyatnykh, A. A. 2000, PASP, 112, 1341
Jerzykiewicz, M., & Wenzel, W. 1977, AcA, 27, 35
Lehmann, H., Harmanec, P., Aerts, C., et al. 2001, A&A, 367, 236
Koen, C. 2006, MNRAS, 371, 1390
Meyer, W. F. 1934, PASP, 46, 202
Sareyan, J. P., Chauville, J., Chapellier, E., & Alvarez, M. 1997, A&A, 321, 145
Sterne, T. E. 1938, ApJ, 87, 133
Wehlau, W., & Leung, K.-C. 1964, ApJ, 139, 843

DISCUSSION

Kovács: What is your opinion about using pure (truncated) Gaussian noise on the observed time base in a Monte Carlo simulations to get an estimate of the noise level?

Jerzykiewicz: It is a useful exercise which may serve as a guide. However, statistical properties of real noise are seldom, if ever, known.

Comm. in Asteroseismology
Vol. 157, 2008, Wrocław HELAS Workshop 2008
M. Breger, W. Dziembowski, & M. Thompson, eds.

Application of the Trend Filtering Algorithm in the search for multiperiodic signals

G. Kovács[1], and G. Á. Bakos[2]

[1] Konkoly Observatory, P.O. Box 67, Budapest H-1125, Hungary
[2] Harvard-Smithsonian Center for Astrophysics, 60 Garden Street, Cambridge, MA 02138, USA

Abstract

During the past few years, the Trend Filtering Algorithm (TFA) has become an important utility in filtering out time-dependent systematic effects in photometric databases for extra-solar planetary transit search. Here, we present the extension of the method to multiperiodic signals and show the high efficiency of the signal detection over the direct frequency analysis on the original database derived by today's standard methods (e.g., aperture photometry). We also consider the (iterative) signal reconstruction that involves the proper extraction of the systematics. The method is demonstrated on the database of fields observed by the HATNet project. A preliminary variability statistics suggests incidence rates between 4 and 10% with many (sub)mmag amplitude variables.

Introduction

The Trend Filtering Algorithm (TFA) has been routinely used during the past several years in the search for transiting extrasolar planets within the HATNet[1] project (Bakos et al. 2004). The goal of this post-processing method is to filter out systematics/trends from the photometric time series. The presence of these effects is due to sub-optimal observing conditions, data acquisition and reduction; e.g., remaining differential extinction, distorted, position- and time-dependent point spread function, astrometric errors, etc. Although wide field observations are the ones most affected by systematics, the fingerprints of these perturbations are always present in nearly all photometric observations (in surveys, such as MACHO – Alcock et al. (2000), or in individual object follow-up observations by small field-of-view telescopes – Kovács & Bakos 2007).

Effects of systematics have not been considered in the past too closely, since, relatively speaking, they play a less important role in large amplitude variables, and most of the earlier investigations focused on specific classes of stars without paying attention to the "constant" stars, displaying the systematics in the most obvious way (due to the lack of more prominent physical variations). This situation has changed with the advent of the microlensing surveys, when it has become clear that more sophisticated image processing tools, such as the image subtraction method (ISIS, see Alard & Lupton 1998) are needed to disentangle weak signals and systematics when searching for variables in crowded fields. While the above differential image analysis works on the images (snapshots of the full photometric time series), TFA (Kovács et al. 2005; hereafter KBN) and SysRem (Tamuz et al. 2005) attempt to utilize the information available in the full time history of the light curves.

[1] **H**ungarian-made **A**utomated **T**elescope **Net**work
http://cfa-www.harvard.edu/ gbakos/HAT/

In the following, we briefly summarize the main steps of the algorithm, extend the method to multiperiodic time series, demonstrate the effectiveness of the method by various tests and perform a brief variability survey on 10 HATNet fields.

TFA with multiperiodic signal reconstruction

Here we briefly summarize the main assumptions and formulae of TFA. The interested reader is referred to KBN and Kovács & Bakos (2007) for additional details.

The basic assumptions are the following: (i) systematics are present in several/many objects in the field (i.e., TFA template selection is possible); (ii) trends in any target are linearly decomposable by using some subset (template) of time series available in the field; (iii) the observed time series is trend- and noise-dominated[2]; (iv) there is a common time base for the large majority of objects. After selecting a set of templates ($\{X_k(i), k = 1, 2, ..., M; i = 1, 2, ..., N\}$ – with k being the template and i being the time index), for each target we compute a filter $F(i)$

$$F(i) = \sum_{k=1}^{M} c_k X_k(i)\,, \tag{1}$$

where the coefficients $\{c_k; k = 1, 2, ..., M\}$ are derived from the following condition for each observed time series $\{Y(i); i = 1, 2, ..., N\}$

$$\sum_{i=1}^{N} [Y(i) - A(i) - F(i)]^2 = min\,. \tag{2}$$

Here the function $\{A(i); i = 1, 2, ..., N\}$ is either constant, or is the trend- and noise-free signal, to be found iteratively in the signal reconstruction phase. For single- and multiperiodic signals, when the Fourier representation of the signal is adequate, we can perform signal reconstruction without iteration. In this case, the Fourier part is included in $F(i)$

$$F(i) \quad = \quad \sum_{k=1}^{M} c_k X_k(i) + \sum_{j=1}^{2L} a_j S_j(i)\,, \tag{3}$$

where $\{S_j(i); j = 1, 2, ..., 2L; i = 1, 2, ..., N\}$ are the Fourier components (*sine* and *cosine* functions) with L different frequencies and $\{a_j\}$ phase-dependent amplitudes. The frequencies are determined from the analysis of a time series derived by Eqs. (1) and (2) with "no signal" assumption (i.e., with $\{A(i) = const\}$). Assuming that these frequencies approximate well the ones representing the noise- and trend-free time series, the advantage of Eq. (3) is that it yields an *exact* solution in one step for signals of the form of *trend + Four. comp. + noise*. If the signal has additional components (e.g., transients, transits) that are not well-represented by a finite Fourier sum, we should use a more complicated model and, as a consequence, an iterative scheme to obtain approximations for the signal components. We note that, in principle, iteration should be employed also if the non-sinusoidal components are absent, because the starting model from which we determine the frequencies is different from the one used in the reconstruction. However, based on our experience from the application of the "no signal" assumption in periodic transit search, the frequencies derived in this way are accurate enough, and there is no need for the very time-consuming iterative procedure in the frequency search.

[2] This property is only used in the frequency search. For signal reconstruction, the full time series model is used, including the hidden signal component.

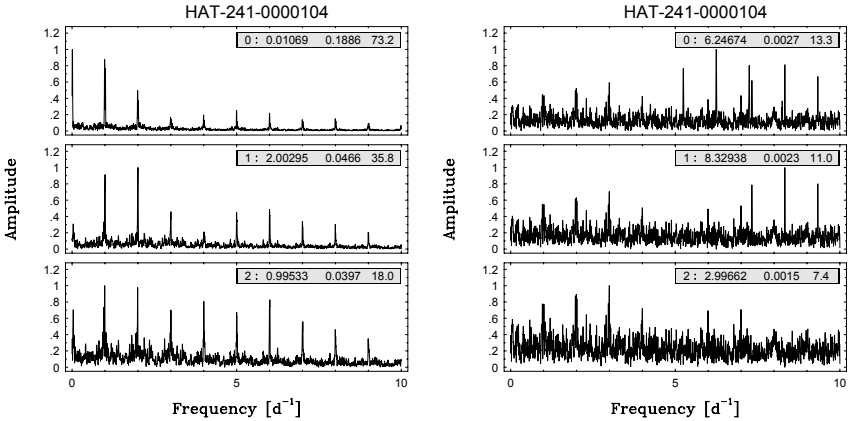

Figure 1: Panels on the left show the successive prewhitening of the *raw test time series* obtained by the injection of two sinusoidal components at 6.25 and 8.33 d^{-1}. Amplitudes are normalized, labels show the prewhitening cycle number, peak frequency, amplitude [mag] and signal-to-noise ratio. Simple Fourier prewhitening cannot recover the signal. Panels on the right show the result obtained by TFA filtering with 900 templates. Both injected signal components are recovered with high significance.

Tests, examples

KBN we presented several tests showing the signal detection capability of TFA on the early set of HATNet light curves, focusing mostly on the detection of periodic transits. Here we show some selected examples on the detection of sinusoidal (i.e., Fourier) signals on the latest, more extensive datasets.

One of the questions that can be asked is why direct Fourier filtering is not used to clean up the data from systematics. The reason is threefold: (i) there are systematics (e.g., transients) for which Fourier representation is a rather bad one; (ii) we do not know *a priori* which component can be treated as a trend and which one as a signal; (iii) for the most common periodic (daily) systematics Fourier filtering is less stable, because of the gaps in the data with the same periodicity. Figure 1 demonstrates the inadequacy of the simple Fourier filtering. The injected low-amplitude signal remains completely hidden if we employ direct Fourier filtering. Although TFA filtering also leaves some trend in the data (see the peak in the bottom right panel at 3.0 d^{-1}), its amplitude is 26-times smaller than that of the highest peak in the direct Fourier filtering at the same stage of prewhitening.

Next, in Fig. 2 we show the frequency spectra of a real variable that has escaped detection in the original time series. The star is rather bright and therefore it is strongly affected by various saturation-related effects. These effects are also common in other bright stars in the field, so it is possible to filter them out by employing TFA. In Fig. 3 we also show the folded light curves to give another look at the difference between the raw and the TFA-reconstructed results. Finally, as an example of the detection capability on the HATNet database, in Fig. 4 we show the frequency spectra of a sub-millimag variable.

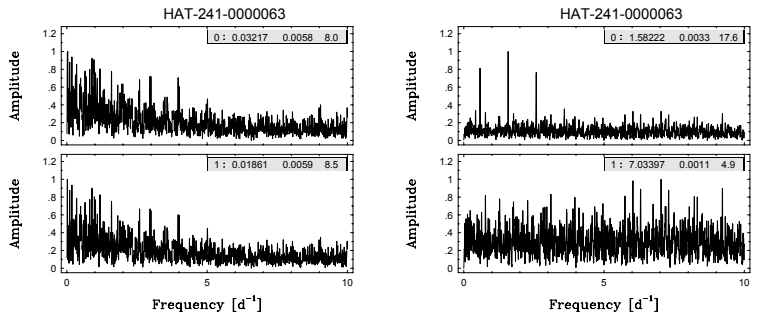

Figure 2: Example on a variable that is hidden in the raw time series (panels on the left) but becomes highly visible in the TFAd time series (panels on the right). Notation is as in Fig. 1.

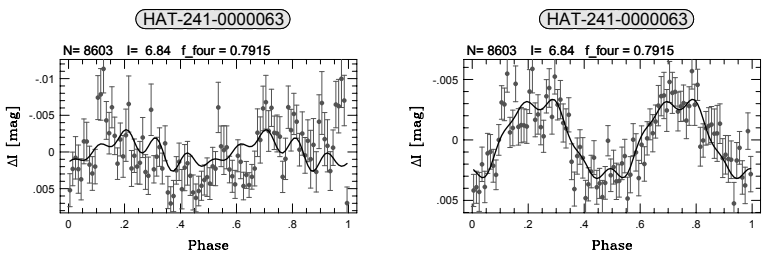

Figure 3: Folded/binned light curves with twice of the period of the variable shown in Fig. 2. Left: raw data, right: TFAd data. Headers from left to right: number of data points, average "I" magnitude, folding frequency in d^{-1}.

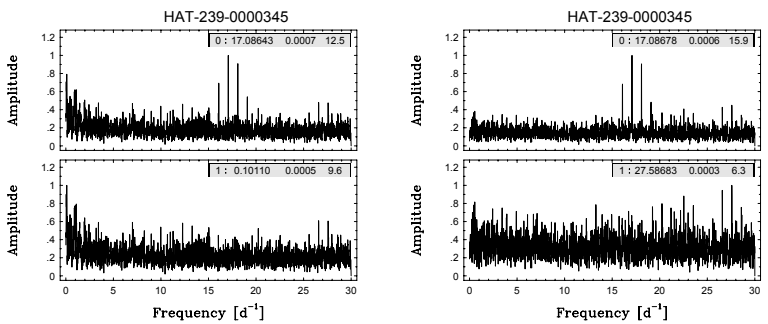

Figure 4: Example on a sub-millimag variable. The signal is detectable also in the raw time series (left) but is cleaner in the TFA filtered one (right). Notation is as in Fig. 2.

Brief HATNet variability statistics

By using TFA post-processing, we have Fourier analyzed 10 HATNet fields in the $[0.0, 20.0]$ d^{-1} range and searched for variables with high significance (SNR$>$ 10) in the frequency spectra. The number of stars analyzed per field varies between 10000 and 25000, with 5000 to 11000 data points per object. The time spans covered by the observations are between 100 and 1000 days. The incidence rates of the variables are between 4 and 10%. The number of sub-mmag variables changes from field-to-field, but it is typically in the order of 100. All these statistics are, of course, strong functions of the data quality, time span of the observations and sample of objects. The total number of objects analyzed is 169000, covering a magnitude range of $7 < V < 13$. The number of variables is 9900. Some 12% of these are sub-mmag variables. For comparison, in an effort to produce a variable input catalog for the Kepler field, Pigulski et al. (2008) analyzed 250000 objects from the ASAS database. They found a variability rate of 0.4%. This low incidence rate is not surprising if we consider that the average number of data points in these ASAS variables is only 100.

Acknowledgments. We thank for the support of the Hungarian Scientific Research Fund (OTKA, grant No. K-60750). Work of G. Á. B was supported by NSF fellowship AST-0702843. Operations of HATNet have been funded by NASA grants NNG04GN74G and NNX08AF23G.

References

Alard, C., & Lupton, R. H. 1998, ApJ, 503, 325

Alcock, C., Allsman, R., Alves, D. R., et al. 2000, ApJ, 542, 257

Bakos, G. Á., Noyes, R. W., Kovács, G., et al. 2004, PASP, 116, 266

Kovács, G., Bakos, G. Á., & Noyes, R. W. 2005, MNRAS, 356, 557 (KBN)

Kovács, G., & Bakos, G. Á. 2007, ASPC, 366, 133

Pigulski, A., Pojmanski, G., Pilecki, B., & Szczygiel, D. 2008, arXiv:0808.2558v2

Tamuz, O., Mazeh, T., & Zucker, S. 2005, MNRAS, 356, 1466

DISCUSSION

Breger: In one of your diagrams, you showed a remarkable improvement in a power spectrum after applying filtering. Could you comment a bit more on the reasons?

Kovács: With a preselected large template set (typically from few hundred to thousand in a field containing $10^3 - 10^4$ objects and similarly large number of data points per photometric time series), we have a good chance to find objects whose light variation contain various parts of systematics present in the target. Systematics have various sources, starting from improper flat-fielding to differential color extinction (see our 2005 paper listed in references for further details).

Comm. in Asteroseismology
Vol. 157, 2008, Wrocław HELAS Workshop 2008
M. Breger, W. Dziembowski, & M. Thompson, eds.

VSAA: A method of tracing variable frequencies in time series analysis

S. Tsantilas, and H. Rovithis-Livaniou

Section of Astrophysics, Astronomy and Mechanics, Dept. of Physics,
Athens University, Panepistimiopolis, Athens, Greece

Abstract

In this work we discuss a new method of time series analysis. This new method -Variable Sine Algorithmic Analysis, (VSAA)- is based on a single sine function with variable coefficients and is powered by the simplex algorithm. It can be applied to almost every type of time series, e.g., to orbital period variations, pulsating stars, sunspot activity, etc., providing a very accurate and simple analysis. Especially in cases of phenomena demonstrating variable frequencies but triggered by a single mechanism, VSAA provides a straightforward solution. Applications are given to synthetic and real data.

Individual Objects: AB And, RR Lyr, Sun

The problem

The periodic nature of certain phenomena is a very common aspect in many scientific fields. likewise in astronomy. A few powerful techniques have been developed in order to analyze the periodic behavior in these cases. The two most common and widely used are the Fourier Transform and the Wavelet Analysis. Fourier Transform (FT) can trace more than one constant frequencies in a time series, but lacks of time-sensitivity. So, if the signal presents a non-constant but quasi-periodic behavior, the FT gives a set of constant frequencies as a result, that should be superimposed in order to describe the original signal. The WA is a more recent method that can produce more time-sensitive results, but the core idea is no different than the Fourier approach. It is like having multiple FT's for consecutive windows. In order to reproduce the original signal, one has to superimpose again all the traced frequencies for each time window.

From the above becomes clear that there is a problem that cannot be handled adequately from the previous techniques: what if we have a time-series presenting a modulated quasi-periodic behavior, but which is triggered by a single mechanism? To demonstrate this problem, we took the case of orbital period variations of the AB And binary system. AB And is a contact binary system of the W UMa type, with masses $m_1 = 0.93 M_\odot$, $m_2 = 0.45 M_\odot$, and orbital period of $P = 0.332$ days. Starting from its O-C diagram and using the First Continuous Method (Kalimeris et al. 1994) we acquired its period variation and we subtracted the long-term variation of 0.006 s/year. This secular increase can be assigned to a number of physical mechanisms like mass transfer. The resulting diagram (Fig.1) represents the actual quasi-periodic variability of the real orbital period of the system.

This diagram can be divided in two parts: The first ranging approximately from 1905 to 1968, and the second from 1969 until today. The first part contains a full 63-year cycle of almost perfect sinusoidal nature and this is the primary frequency detected by the Fourier analysis. But, during the second part, the characteristics of this sinusoidal wave change

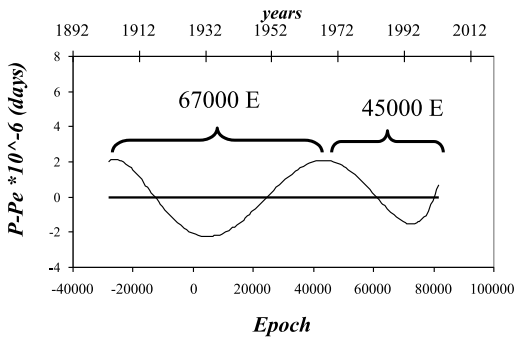

Figure 1: The orbital period variation of the AB And binary

progressively and create a cycle of approximately 39 years with lower amplitude. This makes the orbital period variation of the AB And binary a case that cannot be analyzed by the classic FT or WA. This orbital period variation could be well-assigned to a single mechanism triggered by magnetic activity and described by the Applegate's mechanism (Applegate 1992). Therefore, the need of a new method that can trace this variable frequency and assign it to a single physical mechanism (and not to a superimpose of a huge number of frequencies with no physical explanation) becomes a necessity.

The VSAA Method

The VSAA -Variable Sine Algorithmic Analysis- (Tsantilas & Rovithis 2007) is an algorithmic method accompanied by a computer code, based on the idea of a single sine function with variable coefficients and powered by the **Siplex** algorithm. This way, the output of the analysis is very simple and clear, while the results can be assigned in a straightforward manner to a single mechanism that modulates its characteristics (amplitude and frequency) through time. The core function is:

$$f(t) = a \cdot sin(b \cdot t + c), \tag{1}$$

where $a = a(t)$, $b = b(t)$ and $c = c(t)$, i.e. they are functions of time.
The user has to define some initial values for the following parameters:
a: the amplitude of the signal,
b: the frequency of the signal (multiplied by 2π),
c: the (possible) phase shift,
w: the sliding window width,
it: the number of iterations for every step of the simplex,
acc: the accuracy threshold of the simplex
The user has the option to choose which of the above parameters will be adjustable or fixed. Then, the VSAA starts a partial fit for every window j. The fit is made using the Simplex algorithm (Nelder & Mead 1965). This procedure continues automatically until the end of the time series data set under inspection. The output of the analysis is a set of $N - \ell$ vectors v_j, where N is the number of the input data points and ℓ is an internal parameter that secures that there are enough points in order to have a decent fit. The vectors have the form: $v_j = (t_j, a_j, b_j, c_j, \sigma_j, F_j), j = 1...N - \ell$, where
t_j: denotes the time,
$a_j(t) = \Delta f(t)$: is the amplitude of the variable frequency $f(t)$,

$\frac{b_j(t)}{2\pi} = f(t)$: denotes the variable frequency,
$c_j(t)$: stands for the phase-shift of the function (1),
$\sigma_j = \sqrt{\frac{\Sigma(s_j - F_j)^2}{w}}$ is the mean error, where s_j is the original signal data and F_j is the VSAA fit to the signal.

Applications

Application to synthetic data

In order to be able to evaluate the method and before testing it using real data, we firstly applied it to a synthetic data set (Tsantilas & Rovithis 2008). Obviously, if we know the true solution behind the data set, the program's efficiency can be easily estimated. The data set presents a modulation in amplitude and frequency and includes random error. The excellent VSAA fit is presented in Fig.2a.

Application to the orbital period variation of AB And

The purpose was to analyze the quasi-periodic modulation of the orbital period variation of the AB And and to assign it to a single magnetic Applegate's mechanism. Taking the actual period variation, we firstly subtracted the secular increase produced probably by mass transfer. Therefore, the remaining signal, which is symmetric with respect to the x-axis (a prerequisite for the VSAA, as it is for the Fourier Transform also), could be triggered by the Applegate's magnetic mechanism and is described by the following equation:

$$B^2 \approx 10 \frac{GM^2}{R^4} \left(\frac{a}{R}\right)^2 \frac{\Delta P}{P_{mod}}, \tag{2}$$

where all symbols have their usual meaning; so: M and R denote the mass and the radius of the active star respectively, a stands for the two components separation, B is the intensity of the magnetic field, ΔP and P_{mod} are the amplitude and the period respectively, reported by the VSAA.

Applying the VSAA to this set of data, we acquire the time-dependent frequency and amplitude modulation presented in Fig.2b. Also, with the VSAA and using equation (2), we were able to describe the actual variation of the subsurface magnetic field of the primary component of AB And.

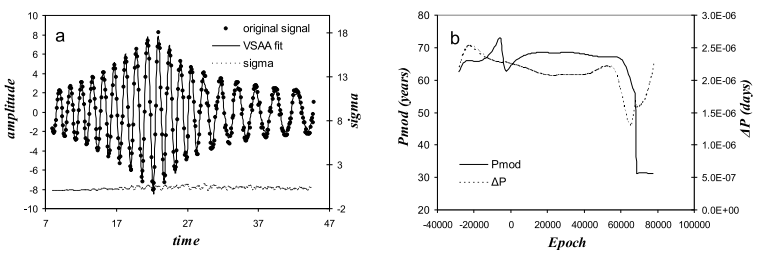

Figure 2: a. VSAA fit on a synthetic data set. b. Period and amplitude variation of the orbital period of the AB And binary

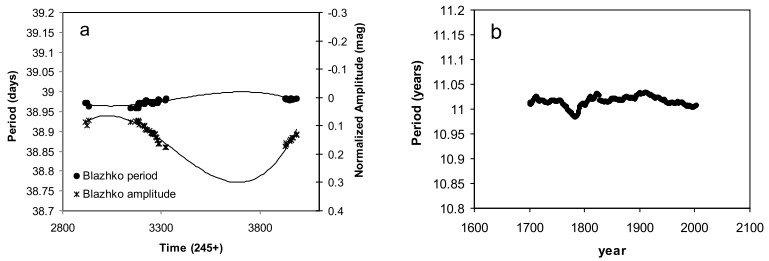

Figure 3: a. Blazhko amplitude and period variation b. Sunspot number period variation

Application to the Blazhko effect of RR Lyr

Given that the mechanism behind the Blazhko effect is not clarified yet, a single-mechanism analysis with the VSAA would be of great interest. As input we used a time-series consisting of the maxima of the RR Lyr light curves from the 2004 survey (Kolenberg et al. 2006) with the addition of some new data from 2006. The resulting Blazhko period and amplitude modulation is presented in Fig.3a. One can observe a smooth variation of the Blazhko period around 38.97 days, while the amplitude demonstrates a second-order sinusoidal modulation. These results are in excellent agreement with previous reports, but offer an additional time-depended insight of the phenomenon.

Application to Wolf's sunspot number

Finally, we applied the VSAA method to the Wolf's sunspot number (Reindel et al. 2008). We used data from the National Geophysical Data Center[1]. The resulting sunspot number period variation can be seen in Fig.3b. A remarkable result from this analysis reflects to the well-known eleven-year solar cycle; for decades, it has been established by various researchers that this cycle is not constant, but presents a certain variability. With the aid of the VSAA, this variability can be traced accurately. Another very interesting aspect of the method is that because the resulting frequency and amplitude are functions of time, we can always have the more recent information about the future trend of the data set. So, the VSAA can be used in order to *predict* the future maximum of the solar cycle, which can be of great importance.

Conclusions

The VSAA can be used very efficiently in many fields of Astrophysics, in order to find non-constant periodicities in time series signals, with the condition that we know (or suspect) that the data set is produced by a single mechanism. The VSAA code, manual and examples, can be downloaded via http at: *http://users.uoa.gr/∼stsant/VSAA.htm*

References

Applegate, J. H. 1992, ApJ, 385, 279
Kalimeris, A., Rovithis-Livaniou, H., & Rovithis, P. 1994, A&A, 282, 775
Kolenberg, K., Smith, H. A., Gazeas, K. D., et al. 2006, A&A, 459, 577
Nelder, J. A., & Mead, R. 1965, Comput. J., 7, 308
Reindel, A., Bradley, P., Tsantilas, S., & Guzik, J. 2008,
GONG 2008/SOHO XXI conference, Boulder, Colorado
Tsantilas, S., & Rovithis-Livaniou, H. 2007, arXiv:0709.3224

[1] (http://web.ngdc.noaa.gov/stp/SOLAR/solar.html)

DISCUSSION

Guzik: Are you able to apply this method to predict sunspots? What would you learn about the mechanism of sunspot formation if this method works?

Tsantilas: Yes! Because of the time sensitivity of the method, it is possible to predict the sunspot number variations. I'm not sure about the level of accuracy of the prediction. Every prediction is risky! I am confident that we can acquire a good picture of what will happen. The output of the code is frequency, f, and amplitude, A, of variations. So, we can compute the A/f ratio.

Michel: What is your justification for fixing the phase shift?

Tsantilas: I have a version in which the phase shift can be variable. Since the solutions in this version are less robust, I consider it better to have the phase shift locked. Also because of the correlation between phase shift and frequency, I believe that the phase shift should be kept fixed.

Baudin: If the phase parameter is kept free, there certainly are some concerns about the uniqueness of the solution.

Tsantilas: Yes, and that is one of the reasons that led us to keep phase shift fixed!

Guenther: Poincaré has shown that in nonlinear systems, to 1^{st} order, only amplitudes and frequencies change. The phase change is a higher order effect, exactly as you have found.

Sotirios Tsantilas and Chloe Vamvatira-Nakou discussing the roofs of Wrocław

Comm. in Asteroseismology
Vol. 157, 2008, Wrocław HELAS Workshop 2008
M. Breger, W. Dziembowski, & M. Thompson, eds.

Asteroseismology of Red Giant stars

N.J. Tarrant, W.J. Chaplin, Y.P. Elsworth, S.A. Spreckley, I.R. Stevens

University of Birmingham, Edgbaston, Birmingham, B15 2TT

Abstract

Sun-like oscillations, that is p-modes excited stochastically by convective noise, have now been observed in a number of Red Giant stars. Compared to those seen in the Sun, these modes are of large amplitude and long period, making the oscillations attractive prospects for observation. However, the low Q-factor of these modes, and issues relating to the rising background at low frequencies, present some interesting challenges for identifying modes and determining the related asteroseismic parameters.

We report on the analysis procedure adopted for peak-bagging by our group at Birmingham, and the techniques used to robustly ensure these are not a product of noise. I also show results from a number of giants extracted from multi-year observations with the SMEI instrument.

Individual Objects: Arcturus, β UMi

Context

Sun-like oscillations - that is to say p modes stochastically excited by convective noise - have now been observed in a number of K-class Red Giant stars (Tarrant et al., 2007, 2008a, Stello et al. 2008). Being of comparably large amplitude relative to other Sun-like oscillators, these oscillations are readily observable. However, the long time series required for the resolution of individual modes is prohibitive for many instruments. Table 1 presents a comparison between the properties of oscillations in the Sun and the range of values expected for a typical K-class giant, based upon the scaling laws of Kjeldsen and Bedding (1995).

In the following sections we discuss the observation of oscillations in K-class giant stars in the context of the study using the SMEI instrument.

Table 1: Comparison of the fundamental parameters of the sun and a K-class giant star.

	Sun	K-class giant
$T_{\rm eff}$ (K)	5777	4000–5000
Luminosity, $L_\odot$	1	20–400
Radius, $R_\odot$	1	5–50
Mass, $M_\odot$	1	0.7–6.0
$\nu_{\rm max}$, (μHz)	3050	0–40
$\Delta\nu$, (μHz)	134.9	0–6
$(\delta L/L)_{700{\rm nm}}$, (ppm)	3.7$\pm$0.2	100–2000

The SMEI instrument

The Solar Mass Ejection Imager (SMEI) instrument (Jackson et al., 2004) is aboard the Coriolis satellite. This satellite occupies a Sun-synchronous polar orbit of period ~ 101 minutes, lying along the day-night terminator. Coriolis was launched on 2003 January 6, entering science mode in the spring of that year. The SMEI instrument was designed to detect transient disturbances in the solar wind by means of imaging Compton scattered light from the free electrons in the solar wind plasma. By this means it is possible to map the heliosphere from 0.4 AU to the Earth, and evaluate the usefulness of sensing the heliosphere as a tool for space weather forecasting.

SMEI comprises 3 cameras, each with a field of view of 60×3 degrees. The cameras are aligned such that the instantaneous total field of view is a strip of sky of size 170×3 degrees; a near-complete image of the sky is obtained from data on all three cameras after every orbit. Individual images – which are made from 10 stacked exposures, with a total integration time of about 40 s – occupy an arc-shaped 1242×256-pixel section of each 1272×576-pixel CCD. Observations are made in white light, and the spectral response of the cameras is very broad, extending from $\sim$ 500 to $\sim$ 900 nm, with a peak at about 700 nm. Here, we give a brief summary of the main steps of the data analysis pipeline used to generate the light curves.

Poor-quality frames having high background are first excluded from any further processing. Processing of the good frames begins with subtraction of bias, calculated from overscan regions at the edges of each frame, and a temperature-scaled dark-current signal. The frames are then flat fielded and spurious signals from cosmic ray hits are removed from the images. The Camera #2 data suffer from some stray light, and further cleaning of these data is performed to minimize the stray-light contribution (Buffington, private communication). The stray-light problem is concentrated in a small number of pixels on the CCD.

Once the images have been cleaned aperture photometry is performed with a modified version of the *DAOPHOT* routines (Stetsen 1987). The target star is tracked, and its light curve is corrected for the degradation of the CCD over the course of the mission, and a position-dependent correction is applied to compensate for variation of the Point Spread Function (PSF) across the frames. When the star lies within the field of view of one of the cameras, a single photometric measurement of its intensity is therefore obtained once every orbit.

In addition to the work on giant stars reported on later in this report, data from these images has been used in studying the period and amplitude evolution of Polaris (Spreckley & Stevens, 2008), and in the discovery of new modes of pulsation in gamma Doradus (Tarrant et al. 2008b).

Issues in analysis

Analysis of time-series data from SMEI is subject to a number of complications and issues, some of which are universally applicable, and some particular to the instrument itself.

Datasets collected from SMEI show significant artifacts at 1 d^{-1} and higher harmonics (as seen in Figure 1). These arise in part as a result of the increased flux of cosmic rays when the satellite passes above the South Atlantic anomaly. An observation will be made once a day while the satellite passes through this region, leading to a higher flux of cosmic rays. As frames with a substantial number of cosmic rays are excluded from the analysis in the pipeline, this introduces a 1 d^{-1} periodicity into the window function. In addition, as the cosmic ray removal process is not perfect, some additional flux from these rays will be present in the photometry, and will contribute a non-sinusoidal flux variation with period one day. A final contribution to the daily artifacts may arise from the stray light issue mention above.

The strength of the daily harmonics in the periodogram is dependent upon the location of a star - for instance the harmonics are of low amplitude in Polaris - and the brightness, with

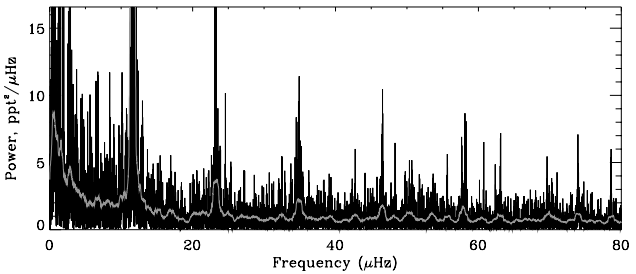

Figure 1: The SMEI periodogram of η Col (HIP 28328, V_{mag}=3.9). Daily harmonics are prominent at 11.57 μHz and multiples. Here the raw transform is shown in black, and a smoothed spectrum is over plotted in grey.

the features becoming more observable at higher magnitudes. These artifacts at the daily cycles restrict the ability to identify oscillatory modes in the regions surrounding 1 d^{-1} and multiples thereof. Fortunately substantial numbers of K-class giants are expected to have oscillations at frequencies lower than 1 d^{-1}, so can be easily differentiated from the the daily harmonics.

In the SMEI data there exists a background which rises steeply at low frequencies, as can be seen in Figure 1. This background consists of the intrinsic variability of the star associated with granulation-noise and active regions of the stellar surface, as well as local processes such as instrumental and photon-shot noise. It is natural to expect that other instruments will have similar backgrounds, although the contribution of instrument noise will vary between observatories, and stellar noise manifests differently between observations made in Doppler velocity and photometry.

A large number of the K-class giant stars are predicted to show oscillations below a few μHz, that is to say in the region where the background begins to rise rapidly. As the statistical tests (see below) for the significance of a feature depend strongly upon the fitted background within the region of a mode, it is essential to accurately model the background noise. As the excess power associated with the modes will itself raise the apparent background level, the region in which excess power is observed may need to be excluded in determining an accurate model of the background.

Considering cases where the modes may be resolved, for many stars the large frequency spacings are predicted to be small, of the order of 1 microhertz. This indicated that a lengthy period of observations is required to resolve the individual peaks of a spectrum. A final issue arises from the lifetimes of modes in giant stars, as manifested in the width of a peak in frequency space. There appears to be an approximate empirical relationship between the Quality-factor (defined here as the frequency divided by the full width at half maximum [FWHM]), and the period of the oscillations (see Figure 2). Considering periods of the giant stars under study, we find that the quality factor for modes can be anticipated to be of the order of 10 to 100, and the FWHM will therefore be of the order of a few tenths of a microhertz. As this width is comparable in size to the expected large frequency separation, we should expect the spectrum to appear very crowded if a significant number of modes are present. In certain cases, this may lead to individual modes being unresolvable. The broad FWHM of these oscillations mean power will be spread across multiple bins in a periodogram. This may mean that no single bin achieves a significant signal-to-noise. In this case, other statistical tests which consider power in multiple bins within a range, e.g., as described below, may be appropriate.

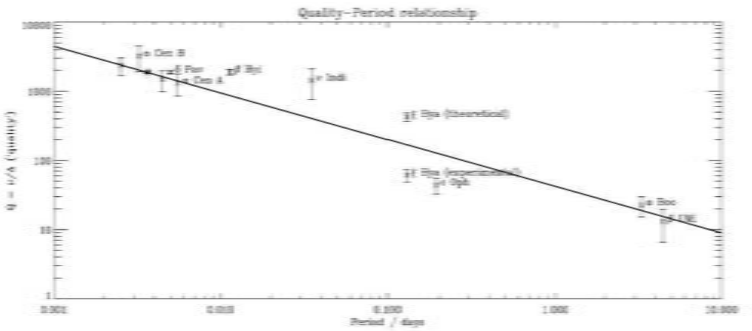

Figure 2: The apparent quality-period relation seen in Sun-like oscillations. The line is a linear fit in log-log space, excluding the theoretical value for ξ Hya. Unlabeled points are two determinations for the Sun using GOLF and BiSON data, and determinations at multiple frequencies for α Cen A and B. (Using values taken from Barban et al. (2007), Bedding et al. (2005), Carrier et al (2007), Houdek and Gough (2002), Kjeldsen et al. (2005) and references therein, Stello et al. (2006), and Tarrant et al. (2007, 2008a))

Analysis Techniques

We first wish to identify the region of excess power (i.e., where the modes are located) in the spectrum, in order that the region can be excluded from the fitting to the background and an estimate of the background level, unprejudiced by the excess power, is derived. We first fit an initial background to the periodogram, choosing one of three models for the background:

1. A power law model of the form $P(\nu) = a + b\nu^{-c}$, reflecting for instance a Brownian noise source.

2. A Harvey model of noise with a memory, consisting of a background and a single component of the form $2\sigma^2\tau/(1 + (2\pi\tau\nu)^2)$, reflecting for instance noise associated with stellar granulation.

3. A Harvey model of noise with memory, consisting of a background and two components, each modelled as in (2), reflecting for instance contributions of both granulation and active regions.

The best fitting background (as determined by likelihood maximisation) is then compared with a smoothed representation of the data, in which the data has been smoothed using a filter consisting of a Gaussian with a FWHM of twice the expected large frequency spacing. Any excess of power will thus be visible as a region where the smoothed profile rises above the background power.

Having thence determined the region in which an excess power is to be found, the background is recomputed with this region excluded from the fitting, again using the three models of the background above. This new background is used to provide the local background level required by the statistical tests described below, and any features which these tests highlight as being significant at a 1% criterion across a range of tests are noted as possible modes. We fit to these features using the full resonant profile of a mode rather than the Lorentzian approximation, as here the Quality-factor is low and this may have an appreciable effect upon the determined mode parameters.

As a final check, and to determine the errors upon fitted values, which may be underestimated by the formal errors, we run a number of simulations of the data, in which we test whether the effects of the window function can reproduce features in the background comparable in significance to those observed.

Statistical Tests

We analyze data by testing whether features can be explained as being a product of a Gaussian-distributed white-noise background. Under these circumstances the normalised power - that is the power over the mean - in a given bin will follow a negative exponential distribution (chi-squared with two degrees of freedom). Where the background is not white, periodogram data can be 'whitened' in the frequency domain by dividing throughout by a model of the local background power.

A number of complementary tests can be applied to data to assess whether a given feature shows a significant deviation of power over the background. The most intuitive of these is to look for single spikes which exceed a threshold in normalised power. However, in the case of K-class giants where the widths of peaks are anticipated to be broad, one can expect for the peaks to be resolved. This opens the possibility of two further tests of significance - considering the power in two or more adjacent bins, and consideration of whether a significant number of bins rise above a threshold value within a small frequency range. A description of the underlying statistics, and how these tests may be applied to periodogram data can be found in Chaplin et al (2002).

In a number of circumstances it may be appropriate to consider the sum of power over a number of adjacent bins. This will enable one to detect broad concentrations of power, in which no single notable spike exists and, when considering ranges greater in size to the large-frequency spacing, to determine the envelope in which a power excess associated with the presence of modes exists, even where individual modes within this region may be unresolved.

Results

Using the above procedures we found a single mode in Arcturus (seen in Figure 1) at a frequency of 3.51 μHz, with an RMS amplitude of 1.23 parts-per-thousand (ppt). These values are in reasonable agreement with predictions based upon the scaling laws of Kjeldsen and Bedding (1995), which predict a frequency of $\nu_{\mathrm{max}} = 4.7 \pm 1.7$ μHz, and an RMS amplitude of 1.3 ± 0.6 ppt.

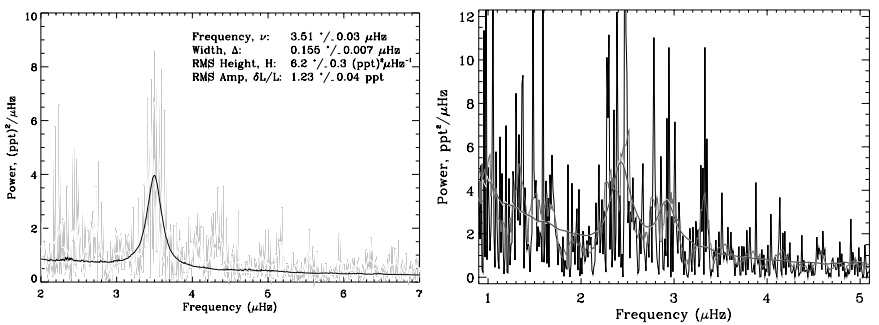

Figure 3: A single significant mode, consistent with scaling laws is seen in Arcturus, while β UMi seems to show a structure of modes.

Table 2: Best-fitting estimates of the identified modes in β UMi.

Frequency (μHz)	Width (FWHM, Δ) (μHz)	Height [(ppt)^2/μHz]	RMS amplitude (ppt)
2.44 ± 0.04	0.2 ± 0.1	5.4 ± 2.2	1.3 ± 0.4
2.92 ± 0.05	0.2 ± 0.1	2.8 ± 1.1	0.9 ± 0.3

In β UMi two features at 2.44 and 2.92 μHz (seen in Figure 1, and described in Table 2) are identified as being statistically significant. Based upon the assumption that these are modes of adjacent radial order, we have determined that these imply a mass for β UMi of 1.3 ± 0.3 $M_\odot$ which differs significantly from evolutionary track and log g mass estimates of 2.2 ± 0.3 $M_\odot$ and 2.5 ± 0.9 $M_\odot$ respectively.

We are in the process of analyzing further giant stars for the presence of individual modes, having noted excesses of power in a number of stars.

Conclusions

The SMEI satellite is a useful tool for observing oscillations in giant stars, although there are certain issues of which the investigator needs to be aware when approaching the data. The use of rigorous statistical tests is an important tool in confirming the presence of the broad features associated with Sun-like oscillations in K-class giant stars.

Given the coverage of the whole sky and long time-series available, SMEI has a valuable rôle to play in the observation of asteroseismic oscillations, not only amongst the K-class giants highlighted here, but also other variables with periods of the order of a few hours to a few days, for instance gamma Doradus and beta Cephei pulsators.

Acknowledgments. The authors acknowledge the support of STFC. SMEI was designed and constructed by USAFRL, UCSD, Boston College, Boston University, and the University of Birmingham NJT would personally like to thank the organizers for arranging this interesting workshop, and HELAS for giving him the chance to present his research.

References

Barban, C., Matthews, J. M., de Ridder, J., et al. 2007, A&A, 468, 1033

Bedding, T. R., Kiss, L. L., Kjeldsen, H., et al. 2005, MNRAS, 361, 1375

Carrier, F., Kjeldsen, H., Bedding, T. R., et al. 2007, A&A, 470, 1059

Chaplin, W. J., Elsworth, Y., Isaak, G. R., et al. 2002, MNRAS, 336, 979

Houdek, G., & Gough, D. O. 2002, MNRAS, 336, 65

Jackson, B. V., Buffington, A., Hick, P.P., et al. 2004, SoPh, 225, 177

Kjeldsen, H., & Bedding, T. R. 1995, A&A, 293, 87

Kjeldsen, H., Bedding, T. R, Butler, R. P., et al. 2005, ApJ, 635, 1281

Spreckley, S. A., & Stevens, I. R. 2008, 388, 1239

Stello, A., Kjeldsen, H., Bedding, T. R., & Buzasi, D. 2006, A&A, 448, 709

Stello, D., Bruntt, H., Preston, H., & Buzasi, D. 2008, ApJ, 674, 53

Stetson, P. B 1987, PASP, 99, 191

Tarrant, N. J., Chaplin, W. J., Elseworth, Y., et al. 2007, MNRAS, 382, 48

Tarrant, N. J., Chaplin, W. J., Elseworth, Y., et al. 2008a, A&A, 483, 43

Tarrant, N. J., Chaplin, W. J., Elseworth, Y., et al. 2008b, A&A, 492, 167

Comm. in Asteroseismology
Vol. 157, 2008, Wrocław HELAS Workshop 2008
M. Breger, W. Dziembowski, & M. Thompson, eds.

An application of Bayesian inference for solar-like pulsators

O. Benomar[1]

[1] Institut d'Astrophysique Spatiale, UMR8617,
Université Paris XI, Batiment 121,91405 Orsay Cedex, France

Abstract

As the amount of data collected by space-borne asteroseismic instruments (such as CoRoT and Kepler) increases drastically, it will be useful to have automated processes to extract a maximum of information from these data. The use of a Bayesian approach could be very helpful for this goal. Only a few attempts have been made in this way (e.g. Brewer et al. 2007). We propose to use Markov Chain Monte Carlo simulations (MCMC) with Metropolis-Hasting (MH) based algorithms to infer the main stellar oscillation parameters from the power spectrum, in the case of solar-like pulsators. Given a number of modes to be fitted, the algorithm is able to give the best set of parameters (frequency, linewidth, amplitude, rotational splitting) corresponding to a chosen input model. We illustrate this algorithm with one of the first CoRoT targets: HD 49933.

Individual Objects: HD 49933

Introduction

Asteroseismology will greatly benefit from the use of data from space-borne instruments. Indeed, MOST and now CoRoT observe stars as no other instruments have done before with high quality and duration. One consequence of this abundance of data is the growing cost of their analysis and higher expectations in terms of inferences on stellar physics. Hence, we need to develop automatic and robust methods to extract information from the data. The Bayesian approach seems to be a promising path to reach this aim because of the possibility to quantitatively take into account *a priori* information.

A star behaves as a resonance cavity and different modes are excited. These resonances appear as peaks in the Fourier spectrum of, for example, the stellar photometric variations. Dealing with solar-like pulsators, we will restrict our analysis to acoustic modes (p modes). These stochastically excited modes are essentially characterised by a frequency, a lifetime and an amplitude. For a power spectrum with a χ^2 distribution with 2 degrees of freedom, Duvall & Harvey (1986) derived the likelihood function for a set of fitted parameters $\boldsymbol{\theta}$, given a model $S(\nu, \boldsymbol{\theta})$ and a power spectrum y,

$$\pi(y|\boldsymbol{\theta}, S) = \prod_{i=1}^{N} \frac{1}{S(\nu_i, \boldsymbol{\theta})} e^{-\frac{y_i}{S(\nu_i, \boldsymbol{\theta})}} \tag{1}$$

where N is the number of frequency samples ν_i. With the Maximum Likelihood Estimator (MLE) approach, the best set of parameters is derived by maximizing the likelihood function (Anderson et al. 1990).

As we want to extract reliably as much information as possible from the data by considering $a\ priori$ information, the Bayesian approach is perfectly suited. Recently, more and more astronomers have begun to use this approach (e.g. Gregory 2005, Parkinson et al. 2006, Brewer et al. 2007, Carrier et al. 2007) in different domains. Applying Bayes rule, we can define a posterior probability density function (pdf). As shown by Appourchaux (2007), in the case of asteroseismic data, the posterior pdf $\pi(\boldsymbol{\theta}|y,S)$ directly depends on the likelihood function $\pi(y|\boldsymbol{\theta},S)$,

$$\pi(\boldsymbol{\theta}|y,S) = \frac{\pi(y|\boldsymbol{\theta},S)\pi(\boldsymbol{\theta}|S)}{\pi(y|S)} \tag{2}$$

where $\pi(\boldsymbol{\theta}|S)$ is a pdf describing our $a\ priori$ knowledge on the parameter set $\boldsymbol{\theta}$. This will be called hereafter the "prior". The denominator is a normalization constant. If we want to apply a prior to a particular parameter (or to a subset of parameters) $\boldsymbol{\theta_k}$, we use the product rule. Let us define $\boldsymbol{\theta} = (\boldsymbol{\theta_k}, \boldsymbol{\theta_{k'}})$, where, for example $\boldsymbol{\theta_{k'}}$ are the amplitudes and $\boldsymbol{\theta_k}$ all the other parameters. The prior $\pi(\boldsymbol{\theta}|S)$ can be rewritten as

$$\pi(\boldsymbol{\theta}|S) = \pi(\boldsymbol{\theta_k}, \boldsymbol{\theta_{k'}}|S) = \pi(\boldsymbol{\theta_k}|S)\pi(\boldsymbol{\theta_{k'}}|\boldsymbol{\theta_k}, S) \tag{3}$$

Assuming that the prior of $\boldsymbol{\theta_k}$ is independent of the prior of any other parameter, we can omit the $\boldsymbol{\theta_k}$ dependence on eq.(3) and rewrite eq.(2)

$$\pi(\boldsymbol{\theta}|y,S) = \frac{\pi(y|\boldsymbol{\theta},S)\pi(\boldsymbol{\theta_{k'}}|S)\pi(\boldsymbol{\theta_k}|S)}{\pi(y|S)} \tag{4}$$

This recipe can be applied as many times as necessary.

In practice, two computation strategies to evaluate the posterior pdf exist:

- Maximum A Posteriori approach (MAP) where we are interested only in the maximum of eq.(4)
- Sampling methods (essentially MCMC algorithms) that provide all of the information on the posterior pdf

We choose the second computational approach for its effectiveness. All the MCMC algorithms consist of a chain of random walks in the parameter space of a function. This allows, MCMC to sample, for example, a pdf whatever the complexity of the analytical form of the function. Moreover, compared to gradient methods widely used to find the maximum of a function, MCMC are insensitive to the departure point in the space of parameters. This means that the initial $\boldsymbol{\theta}$ vector can be set arbitrarily yielding nevertheless a proper sampling around the maximum. In consequence, if multiple maxima exist, the algorithm will not miss the true maximum of the function (under some conditions detailed in Section 2). MCMC also enables numerical integration widely used in the Bayesian approach. Let us introduce some basic aspects of the MH algorithm (Metropolis et al. 1953, Hastings 1970). Considering an equilibrium distribution (the function that we want to sample) $\pi(\boldsymbol{\theta})$, we define a probability transition function $\alpha(\boldsymbol{\theta_{i+1}}, \boldsymbol{\theta_i})$ from an initial parameter set $\boldsymbol{\theta_i}$ to a new proposed set $\boldsymbol{\theta_{i+1}}$, in order to sample the space of parameters

$$\alpha(\boldsymbol{\theta_{i+1}}, \boldsymbol{\theta_i}) = min\{1, \frac{\pi(\boldsymbol{\theta_{i+1}})q(\boldsymbol{\theta_{i+1}}|\boldsymbol{\theta_i})}{\pi(\boldsymbol{\theta_i})q(\boldsymbol{\theta_i}|\boldsymbol{\theta_{i+1}})}\} \tag{5}$$

where $q(\boldsymbol{\theta_i}|\boldsymbol{\theta_{i+1}})$ is the proposal pdf of transition. Hence, it is related to the step size of the transition. If q is symmetrical, then the ratio $\frac{q(\boldsymbol{\theta_{i+1}}|\boldsymbol{\theta_i})}{q(\boldsymbol{\theta_i}|\boldsymbol{\theta_{i+1}})}$ reduces to 1. Usually q is chosen to be a Gaussian distribution. This choice is not necessarily the best but the simplest one (Roberts & Rosenthal 2001). The quantity α is compared to a uniform random variable $u \in [0,1]$. If the ratio $\frac{\pi(\boldsymbol{\theta_{i+1}})q(\boldsymbol{\theta_{i+1}}|\boldsymbol{\theta_i})}{\pi(\boldsymbol{\theta_i})q(\boldsymbol{\theta_i}|\boldsymbol{\theta_{i+1}})}$ is greater than 1, the transition from $\boldsymbol{\theta_i}$ to $\boldsymbol{\theta_{i+1}}$ is always accepted. Otherwise, the move is accepted with a probability equal to the ratio.

Algorithm details

Choice of the covariance matrix of the proposal distribution

Assuming that the proposal distribution $q(\boldsymbol{\theta_{i+1}}|\boldsymbol{\theta_i}) = N(\boldsymbol{\theta_i}, \boldsymbol{\Sigma})$ is a Gaussian centered on $\boldsymbol{\theta_i}$ and of variance $\boldsymbol{\Sigma}$, the only parameter that we have to scale is the covariance matrix $\boldsymbol{\Sigma}^{-1}$ of this distribution. The choice of $\boldsymbol{\Sigma}^{-1}$ affects the acceptance rate and hence the sampling efficiency. If the acceptance rate is too high, too many transitions are accepted which results in unnecessarily small steps in the parameter space. The risk of sampling a local maximum rather than the global pdf is high. A low acceptance rate corresponds to large proposed step transitions and to an excessively low sampling rate. Following Atchadé (2006), the best sampling is obtained for an acceptance rate between 0.2 and 0.5. To have a flexible algorithm, we choose to use a self-learning process that adapts the covariance matrix according to the data. Even the correlation between parameters is taken into account (nondiagonal matrix). It can be argued that this kind of algorithm violates the Markovian nature of the sampling process. This is true, but, in fact, one can stop the learning process when the acceptance rate is satisfactory.

Parallel tempering

When the posterior pdf has multiple local maxima (e.g. when sampling the sum of 2 Gaussian distributions), MCMC can be trapped in one of these maxima, especially if they are far from one another in the parameter space. Indeed, the probability transition $\alpha(\boldsymbol{\theta_{i+1}}, \boldsymbol{\theta_i})$ is close to 0 between two distant maxima. A solution to avoid this problem and to efficiently sample all of the parameter space was first suggested by Jennison (1993). It consists in launching k different MCMC in parallel. Each MCMC has a different equilibrium distribution

$$\forall i \in [1, k], \pi_i(\boldsymbol{\theta}) \propto \pi(\boldsymbol{\theta})^{1/T_i} \tag{6}$$

where T_i is called the temperature of the chain. The higher the temperature is, the lower is the potential barrier between two local maxima. Applying a temperature is like "stretching" the distribution of interest (compared to the colder chain $\pi_1(\boldsymbol{\theta})$). The displacement in the space parameter are easier at high temperature than at low temperature. We choose a geometrical law for the temperature profile

$$T_i = \lambda^{i-1} \tag{7}$$

where λ is a scaling factor. At each iteration, j, we mix two adjacent and randomly chosen chains, i and $i+1$ with a probability

$$\alpha(\boldsymbol{\theta_i^{(j)}}, \boldsymbol{\theta_{i+1}^{(j)}}) = min\{1, \frac{\pi_i(\boldsymbol{\theta_{i+1}^{(j)}})\pi_{i+1}(\boldsymbol{\theta_i^{(j)}})}{\pi_i(\boldsymbol{\theta_i^{(j)}})\pi_{i+1}(\boldsymbol{\theta_{i+1}^{(j)}})}\} \tag{8}$$

Then all of the values can be discarded except those related to the distribution of interest (i.e. for $\pi_1(\boldsymbol{\theta})$). λ is adjusted to ensure an acceptance rate around 50%.

Condition to stop the sampling

In the MH algorithm, the number of samples to compute is difficult to set . When can we assume that all of the region of interest (i.e. where π is not close to zero) of the parameter space has been visited? This question is still discussed in the literature. Different authors proposed indicators to stop the sampling (see the review of Brooks & Roberts 1998). The simplest one consists in monitoring the posterior probability parameters and assuming the steady state to be reached when the parameter mean value and rms error are stable.

Physical assertion and Bayesian considerations in the case of solar-like pulsators

For a single mode, the mean power spectrum can be described by a sum of Lorentzian profiles plus background noise. As we wish to make a global fit including several modes expected in a wide frequency range, we should use the general relation

$$S(\nu,\boldsymbol{\theta}) = \sum_{n=n_0}^{N_{\max}} \sum_{l=0}^{L_{\max}} \sum_{m=-l}^{+l} \frac{A_{n,l,m}}{(1+\frac{\nu-\nu_0+ms}{\Gamma_{n,l,m}/2})^2} + \frac{B_0}{1+B_1\nu^p} + B_2 \tag{9}$$

where $A_{n,l,m}, \nu_{n,l,m}, s, \Gamma_{n,l,m}$ are the height, the central frequency, the rotational splitting and the linewidth at half maximum, respectively. B_0, B_1, B_2, p are parameters associated with the noise profile, chosen to be the sum of Harvey-like profiles plus white noise (Harvey 1985). In the solar-like pulsator case and in the asymptotic approximation, the central frequency of a set of modes (n, l) is approximately given by the relation

$$\nu(n,l) \approx \Delta\nu(n+l/2+\epsilon) - l(l+1)D_0 \tag{10}$$

with $\Delta\nu = \nu_{n+1,l} - \nu_{n,l}$ and D_0 are related to the sound speed at differents depths. The large separation $\Delta\nu$ is related to the mean stellar density and D_0 to more local properties. Eq.(10) can be used as a strong prior on the frequency dispersion. Indeed, the large separation estimation is easy (e.g. from the spectrum autocorrelation) and D_0 can be constrained by a previous modelisation of the star.

Application to HD 49933

Prior definition

We applied our algorithm to a CoRoT target, HD 49933, continuously observed for 60 days. This star was previously analyzed by Mosser et al. (2005) and more recently by Appourchaux et al. (2008). The autocorrelation of the power spectrum gives us a precise estimate of the large separation: 85.6 ± 0.8 μHz. We choose a Gaussian prior for the large separation according to these values. The low S/N ratio prevents a clear detection of the l=2 modes, even in an echelle diagram. D_0 is around 1 μHz (Appourchaux et al. 2006) according to stellar models. This leads to a frequency difference between l=0 and the neighboring l=2 modes of $\delta_{02} \simeq 6\mu$Hz. The tolerance should be large as we do not have a lot of confidence. So we define a Gaussian prior with $\delta_{02} = 6 \pm 2.5$ μHz.

The *a priori* information on the rotational splitting is extracted from the very low frequency part of the power spectrum. A peak which is supposed to be due to transiting structures on the stellar surface appears at 3.4 μHz. We choose a one-σ tolerance of 10% of this value.

The angle between the line of sight of CoRoT and the star's rotation axis is an important parameter for p-mode analysis in the power spectrum, as it affects the relative amplitude of the split components of nonradial modes (Gizon & Solanki 2003). Estimates (from *v.sini* measurement, radius and rotation estimation) give a probable angle of 26 ± 4 °, but there is a substantial discrepancy with the asteroseismological interpretation leading to an angle between 50 and 62 degrees (Appourchaux et al. 2008). In order to avoid any prejudice, we decided to use a weak prior: a uniform prior probability, from 15 to 70 degrees.

For all others parameters, the only prior consists in allowing only real positive values. The defined priors are improper and uniform. Moreover, to increase the fit stability, we fit a single linewidth by large separation and consider 15 radial orders in the frequency range 1200 - 2600 μHz. Finally, we deal with 81 parameters.

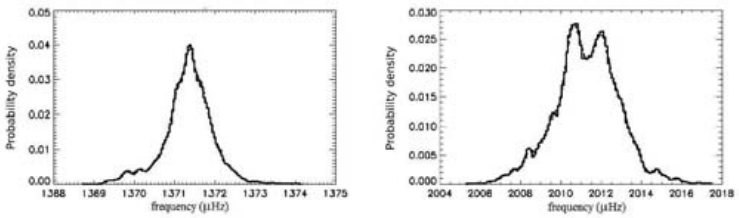

Figure 1: Example of pdf vs. frequency for the CoRoT photometry of HD 49933. Left : monomodal distribution ($l = 1$). Right : bimodal distribution ($l = 2$)

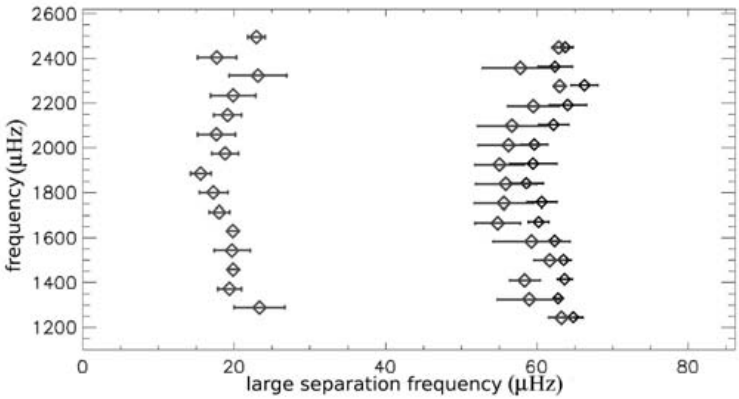

Figure 2: Echelle diagram. Error bars represent 3-σ errors. On the left $l = 1$, on the right $l = 2$ and $l = 0$

Results from the global fit

200000 samples had to be computed before reaching the steady state. The estimated value for the splitting is 3.0 ± 0.2 μHz. This suggests a lower rotational velocity for the inner parts of the star compared to the surface. The inclination is evaluate to be 46 ± 6 °. The large separation is 86.2 ± 0.2 μHz. The values for these three parameters confirm those found by Appourchaux et al. (2008) using MLE. One of the main differences comes from the frequency estimation for $l = 2$ modes. Our values are constrained by the $a\ priori$ information and avoid negative δ_{02} values (see Fig.2). Some parameter pdfs are clearly multimodal (see Fig.1), especially for the $l = 2$ mode central frequencies which have amplitudes close to the noise level (S/N around 1).

Conclusion

We presented an analysis method based on MCMC and Bayesian inference. These methods show many advantages compared to the more classical one used in asteroseismologic data analysis: The sampling capabilities of Markov Chains Monte Carlo (MCMC) provide full information on the probability density function (pdf) of the parameters and not only a maximum of

the probability. Hence, a multimodal pdf is not a problem. Moreover, the adaptive capacities of MCMC permit us to envisage the development of automatic fitting procedures. As shown, thanks to $a\ priori$ information, the Bayesian inference has the capacity to extract more realistic parameters from data than Maximum Likelihood Estimator approach (MLE). Compared to a simple likelihood estimator, the reliability is increased. Of course, the data quality is a limit and we have to be careful not to introduce too strong priors. The results presented for CoRoT photometry of HD 49933 confirm the angle inclination value and rotational splitting found by the MLE approach. They also show that the pdfs are multimodal in some cases, as for the $l = 2$ frequencies and explain the failure of MLE methods to find the true maximum of probability. The main reason is that the S/N is low, increasing the occurence of multimodal pdfs.

Acknowledgments. I acknowledge T. Appourchaux for his explanations on the fitting methods and Bayesian inference. I would also like to thank F. Baudin for his regular assistance in my work. Many thanks also to an anonymous referee for his detailed reading which has resulted in great improvements.

References

Anderson, E. R., Duvall, T. L. J., & Jefferies, S. M. 1990, ApJ, 364, 699

Appourchaux, T., Michel, E., Auvergne, M., et al. 2008, A&A, 488, 705

Appourchaux, T., Berthomieu, G., Michel, E., et al. 2006, ESA SP-1306, 429

Appourchaux, T. 2008, AN, 329, 5, 485

Atchadé, Y. F. 2006, Meth. Comp. In Applied Probab. 8, 235

Brewer, B. J., Bedding, T. R.,Kjeldsen, H., & Stello, D. 2007, ApJ, 654, 551

Brooks, S. P., & Roberts, G. O. 1998, StCom, 8, 319

Duvall,T. L., Jr., & Harvey, J.W. 1986, ssds,105

Carrier, F., Kjeldsen, H., Bedding, T. R., et al. 2007, A&A, 470, 1059

Gizon, L., & Solanki, S. K. 2003, ApJ, 589, 1009

Gregory, P. C. 2005, ApJ, 631, 1198

Harvey, J. 1985, ESA SP-235, 199

Hasting, W. K. 1970, Biome 57, 97

Metropolis, N., Rosenbluth, A. W., Rosenbluth, M. N., et al. 1953, J. Chem. Phys., 21, 1087

Mosser, B., Bouchy, F., Catala, C., et al. 2005, A&A, 431, L13

Jennison, C. 1993, JRSSB, 55, 54

Parkinson, D., Mukherjee, P., & Liddle, A. R. 2006, PhRvD, 73, 123523

Roberts, G. O., & Rosenthal, J. S. 2001, Statist. Sci., 16, 351

Poster session

Andrzej Pigulski and Paweł Moskalik